Desalination and Water Treatment
www.deswater.com
1 (2009) 128–138
1944-3994/1944-3986

Experiment and optimal parameters of a solar heating system study on an absorption solar desalination unit

Chen Ziqian[a,b], Zheng Hongfei[a*], Ma Chaochen[a] ,Li Zhengliang[c], He Kaiyan[a,b]

[a]*School of Mechanical and Vehicular Engineering, Beijing Institute of Technology, Beijing 100081, China*
Tel. +86 10 6891 2510; Fax: +86 01 6894 9859; email: hongfeizh@bit.edu.cn
[b]*School of Physics, Science and Technology, Guangxi University, Nanning, Guangxi 530004, China*
[c]*Physics Department, Guangxi Teacher College, Nanning, Guangxi 530001, China*

Received 24 November 2006; Accepted 21 August 2008

ABSTRACT

Based on the mechanism of falling film evaporation and condensation, a quadruple effect regeneration absorption solar desalination unit was designed and tested indoors under transient and steady-state conditions. The performance ratio and the flow rate of freshwater of the unit at different operating temperature and pressure were studied. Through the test, it is shown that the performance ratio of the unit is high because most of latent heat of vapors and part of sensible heat of brine are utilized many times. Meantime, lithium bromide can automatically absorb the vapors of the last stage evaporator so as to recover vapor enthalpy and intensify the process of evaporation. The PR of the unit is more than 3.0, which illustrates the advantages of the absorption desalination system. The other factors influencing the flow rate of freshwater were also researched. From the indoor experimental results, the solar heating system of the unit was studied by simulation under the conditions of the least cost of fresh water. The optimal parameters, which are solar collector areas, storage volume, start-up and break temperatures, are given.

Keywords: Solar desalination; Falling evaporation; Absorption

1. Introduction

Multi-stage flash, multi-effect distillation, reverse osmosis, electrodialysis and vapor compress desalination have been the conventional desalination technology for a long time [1]. With the further recognition of the people on the relationship among desalination and the environment and the shortage of fossil-fuel energy, the use of renewable energy and research of new desalination technology are being given more prominence [2].

A new process was proposed by Weinberg et al. [3] in 1980. The process is integrating the multi-effect desalination system with a vacuum freezing unit utilizing a LiBr–H_2O solution, which can increase the economy ratio of the proposed unit to the high values of 18 to 20. Fathalah and Aly [4] analyzed the combination of a multi-effect desalination system and a LiBr–H_2O heat pump operated by solar energy. A1-Juwayhel et al. [5] had researched the performances of single-effect evaporator desalination systems combined with vapor compression heat pumps.

Although the studies on absorption desalination systems have been reported many times, the commercialized and industrialized units have not yet been found [6]. Therefore, further research on this kind of unit seems to be useful. On the other hand, the optimization study of the solar desalination unit is very important and helpful for people to know how to reduce the cost of the fresh water production. García-Rodríguez et al. [7] and El-Nashar [8] studied the optimization of a solar multi-effect distillation system. On the basis of the thermoeconomic analysis of the Sol-14 plant, which is a solar multi-effect distillation

*Corresponding author.

system installed at the Plataforma Solar de Almerla in southeastern Spain, García-Rodríguez et al. studied the correlations of distilled water costs with the cost of thermal energy and the performance ratio with the product cost, the influences of the inlet/outlet temperatures of the thermal oil in the solar field on the cost of the exergy supplied to the desalination plant as well as the annual production of the solar desalination system and the distillation plant capacity on the distilled water cost, respectively. Also, García-Rodríguez et al. studied the Sol-14 plant that was connected with six different kinds of solar systems and compared the results [9]. El-Nashar had developed the "SOLDES" simulation program after having researched the solar desalination plant in Abu Dhabi for a long time [10]. The program can be used to simulate the operation of a solar desalination plant which is composed of evacuated tube collectors, heat accumulators and a multi-effect distillation system.

As a result of this study, an absorption solar desalination unit in which multi-stage falling film evaporation and condensation as well as other intensified heat and mass transfer processes were utilized, was designed. Firstly, the transient and steady-state performances of the unit were tested indoors by simulating solar heating system with an electrical heater and the performance ratio and yield rate under the conditions of different operating temperatures and pressures were studied. Secondly, the solar heating system of the unit was simulated by utilizing the results of an experimental study under steady-state conditions and the metrological data to study the optimal parameters of the solar heating system. In this work, unlike the optimization studies of García-Rodríguez and El-Nashar, it takes the solar desalination unit as a system which is composed of two subsystems. The two subsystems are a solar heating system and an absorption solar desalination system. With the help of single-factor analysis, the four parameters, which are solar collector area, storage capacity, start-up and break temperatures of the absorption solar desalination system, are discussed and optimized simultaneously.

2. Description of the main components of the unit

The unit is mainly composed of solar heating and absorption desalination systems. The schematic diagram of the unit is shown in Fig. 1. The absorption desalination system, which includes an absorber, a generator, four evaporators, a heat exchanger, two storages and other parts, was tested indoors by substituting the solar heating system with electrical heater.

Generator and absorber: Both look like the same in their structures and dimensions. But there is one more steam inlet in the absorber than that in the generator (see Fig. 1). There is a shell and tube heat exchanger with a 400 mm inner diameter and 1200 mm height on the inside of the generator and absorber respectively. The exchangers are composed of 43 vertical tubes with inner and outer diameters of 28 and 32 mm, 750 mm length. Hence the inner and outer heat exchanger areas are 2.84 and 3.24m^2 respectively. For enhancing the effect of heat transfer and completely wetting the wall of the tubes, a spiral wire with a 2.5 mm diameter and 2 m length is inserted in each tube. The wire makes contact with the inside wall of the tube because of its tension force, which is helpful to intensify the effects of falling film evaporation and condensation.

There is a round sprayer on the upper part of generator and absorber. The diameter, height and holed diameter of the sprayer, the intervals between the holes and the distance from the sprayer to evaporation tubes are 360 mm, 30 mm, 2 mm, 2 mm×2 mm and 25 0mm, respectively.

Four evaporators: There are four evaporators with the same structures, which can be equipped or combined into a double, triple or quadruple effect system. The outer height, length and width of the evaporators are 800 mm, 500 mm and 500 mm. Each evaporator has 56 horizontal brass tubes with the inner and outer diameters of 28 and 32 mm, 450 mm length. The total inner and outer areas of the tubes in an evaporator are 2.22 and 2.53m^2 respectively. The tubes are traversed and crosswise arranged between different layers so as to assure each droplet of brine dropped on the outside wall of evaporation tubes and form falling film.

There is a rectangular sprayer on the upper part of every evaporator. Its bottom dimensions and height are 460×460 mm and 30 mm. The diameter of the holes on the sprayer, intervals between holes and distance from the sprayer to the evaporation tubes are 2 mm, 2 mm×2 mm and 200 mm, respectively.

Heat exchanger: The heat exchanger consists of coaxial tubes in which the hot solution flows in the inner tube. The total area of heat exchange is 0.138 m^2.

Other components: The plastic–aluminum pipes with diameters of 15 mm and 20 mm were used with a lithium bromide solution and water (including brine and fresh water) pipes in the experiment, respectively. The diameter of steam pipes is 60 mm.

3. Operational principle of the unit

As shown in Fig. 1, seawater is pumped into the absorber (27) from the inlet (31) and some of the sea water will flow into the every evaporator as feedstock via water pipe (25) and flowmeters (9) after passing through the outside walls of the vertical tubes in the cavity of the absorber (27). The rest of the sea water will be discharged from the outlet (23).

The seawater in the evaporators is pumped into the sprayer via pumps (7) and sprayed on the outer walls of

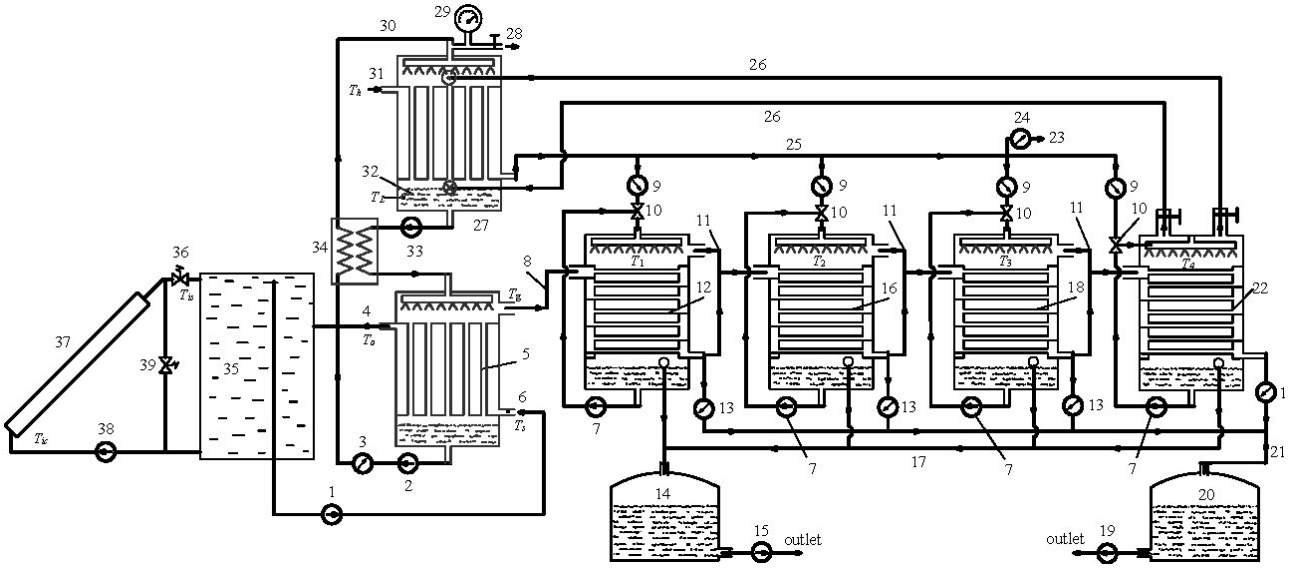

Fig. 1. Schematic diagram of the unit. 1 circulation water pump; 2 LiBr–H_2O solution circulation pump; 3 LiBr–H_2O solution flowmeter; 4 hot fluid outlet; 5 generator; 6 hot fluid inlet; 7 circulation water pump; 8 heated steam pipe; 9 feedstock flowmeter; 10 adjusted valve; 11 vapor pipe; 12 first-stage evaporator; 13 freshwater flowmeter; 14 condensed brine storage; 15 condensed brine pump; 16 second-stage evaporator; 17 condensed brine pipe; 18 third-stage evaporator; 19 freshwater pump; 20 freshwater storage; 21 freshwater pipe; 22 fourth-stage evaporator; 23 cooling seawater outlet; 24 cooling seawater flowmeter; 25. seawater pipe; 26 vapor pipe; 27 absorber; 28 vacummizing outlet; 29 vacuometer; 30 LiBr–H_2O solution pipe; 31 seawater inlet; 32 LiBr–H_2O solution; 33 LiBr–H_2O solution circulation pump; 34 heat exchanger; 35 hot water storage; 36 by-pass valve; 37 solar collectors; 38 circulation water pump; 39 by-pass valve.

the horizontal tubes where the seawater becomes falling film and is evaporated. The condensed brine flows into the storage (14) via pipe (17) with respect to gravity and is pumped out by pump (15) from the outlet of the storage (14).

The LiBr–H_2O solution in the absorber (27) absorbed the steam from the fourth-stage evaporator (22) and became diluted. The diluted solution is pumped through the heat exchanger (34) by a pump (33) where its temperature increases, and is sprayed in generator (5) so as to enhance the efficiency of absorption with the help of the process of falling film absorption. The heat supplied to generator (5) is from solar heating system or simulator.

The hot steam produced in generator (5) flows into the inside of the horizontal tubes in the first-stage evaporator (12) and releases the latent heat to the falling film of seawater on the outside of the horizontal tubes, which makes the temperature of the film increase and the film evaporate. At the same time, the vapor in the inside of the tubes is condensed into fresh water which flows into fresh water storage (20) via pipe (21) and is pumped out (19) from the outlet of the storage (20). The LiBr–H_2O solution is condensed and evaporated in a generator (5). Then the condensed solution is recycled into the absorber (31) to absorb the vapor again after passing through the heat exchanger (34). The system repeats the circulation continuously.

The vapor produced on the outside of the horizontal tubes by falling film evaporation in the first-stage evaporator (12) enters the inside of the second-stage evaporator (16) and releases the latent heat to the falling film of sea water on the outside of the horizontal tubes, which increases the temperature of the film and it is evaporated again. Meanwhile the vapor in the inside of the tubes is condensed into fresh water which flows into fresh water storage (20) via pipe (21) and is pumped out (19) from the outlet. The system operates repeatedly in this way that the vapor produced in the preceding evaporator is conveyed into next evaporator to produce fresh water and releases latent heat again. It lets the heat entering the system be recycled many times. The fresh water produced in every evaporator is collected in the storage (20) via the pipe (21).

The heat exchanger (34) between the absorber (27) and generator (5) is used to preheat the diluted solution which flows into the generator (5) from the absorber (27). Meantime the condensed solution which enters the absorber (27) is cooled and part of the heat is recycled.

The evaporated vapor in the last evaporator (22) is driven into the absorber (27) in which the vapor is absorbed by lithium bromide and releases the latent heat to the seawater which flows inside the absorber (27) and the temperature of the water increases, due to the difference of vapor pressure between the absorber (27) and last evaporator (22). Then in absorber (27), the sea water from

the inlet and part of the heat from the last evaporator (22) is preheated and recycled respectively.

The lower pressure required by the system is maintained by a vacuum pump.

When the solar collectors (37) absorb the solar radiation and transform it into thermal energy, the collector fluid is heated. As soon as the temperature of the collector fluid increases to a certain value, the valve (36) is open and the by-pass valve (39) is closed so as to pump the fluid into the storage (35). If the temperature of collector fluid is lower than the certain value, the by-pass valve (39) is open and the valve (37) is closed so as to heat the fluid in the collectors by circulation. Whether the circulation water pump (38) being on or off is controlled by a solar controller. After comparing the temperature of collector fluid and the environment and it is found that the irradiance is strong enough to increase the temperature of collector fluid, the pump (38) is on, otherwise off. The highest temperature of system is designed to be 115°C. The storage (35) connects with solar collectors to the absorption desalination system. The fluid in the storage (35) flows to the generator (5) and back after exchanging heat with the lithium bromide solution there.

4. Measurement of the experimental data

The temperatures T_g, T_h, T_L, T_o, T_s and T_1–T_4 (in Fig. 1) were read by computer through the signal provided by the thermocouples located at the measurement points, which had been demarcated with the accuracy of ±0.1. The uncertainty was less than 1%. The ambient and the brine temperatures were measured with a common glass-tube mercury temperature thermometer. The absolute deviation of the temperature was less than 0.5°C.

The fresh water yield in every evaporator was read through the flowmeter and the experimental data were record every 10 min. The fresh water yield of the system was the sum of fresh water yields in every evaporator. The relative error was 5%.

The flow rates of the feedstock, hot and cooling water, and the circulation water in each evaporator were measured every 10 min by water meters. The experimental data were the averages of many measurement results. The flow rate of feedstock entering each evaporator could be adjusted by a valve. The absolute and relative deviations of the flow rates of hot and cooling water were ±50 kg/h and 5%, respectively.

During the period of the experiment, the solar heating system was replaced by three electric heaters and the temperature of the hot water was about 65–95°C. The ambient temperature and humidity were relatively steady during the experimental period. They were 20–25°C and 40–85% respectively. The brine in the experiment was the city water. Electrical power was required for the hot and cooling water circulation pumps as well as a vacuum pump. The total power was 1300 W.

5. Steady-state experimental results and discussion

The performance of the system under steady-state conditions was studied through indoor experiments. The flow rates of the feedstock, heating and cooling water, and the circulation water in each evaporator were 40–80, 820±50, 600±30 and 240–280 kg/h, respectively. The operating pressure P in the absorber (called operating pressure hereafter) was 10 kPa and the temperature of cooling water entering the system was 18±0.5°C.

When the hot water was heated to a certain value, the system started operating and the yield was recorded every 10 min. The temperatures were recorded by computer automatically.

When the temperature of hot water was heated by an electrical heater to 75°C, the hot water started to flow into the generator. The variation curves of freshwater yields of every evaporator and their sums every 10 min with the operating time are shown in Figs. 2 and 3.

As shown in Figs. 2 and 3, the total yield of the system per 10 min will be steady after about 40 min of operation, even if the yield rates of fresh water in the third and fourth stages do not achieve the maximum. It can be seen in Fig. 3 that the yield rates of the first and second stages achieve the maximum after about 40 min of operation and decrease slightly and then remain steady. The yield rates of the third and fourth stages obtain steady value until 60 min later. The slight decreases of yield rates of the first and second stages after achieving the maximum may be explained as that the temperature of next stage evaporator was lower at the beginning. It was helpful for evaporating in the preceding stage evaporator; then the yield rates increased quickly. However, with the increase of the temperature of the next stage evaporator, the resistance of heat transfer increased. It was unfavorable for evaporating in the earlier stage evaporator and then the yield rates decreased.

Fixing the operating conditions as the foregoing, the temperature variations of T_g, T_1, T_2, T_3 and T_4 with the operating time are shown in Fig. 4. It can be seen that the temperatures T_h, T_L, T_o, T_s and others are basically steady after the system operated for 60–80 min.

When the operating pressure and heating and cooling water rates are 10 kPa, 820±50 and 600±30 kg/h, respectively, the variation of the total yield per hour with the operating temperature is shown in Fig. 5. It can be seen that the yield increases with the raise of operating temperature and the equation of the variation curve can be fitted as follows:

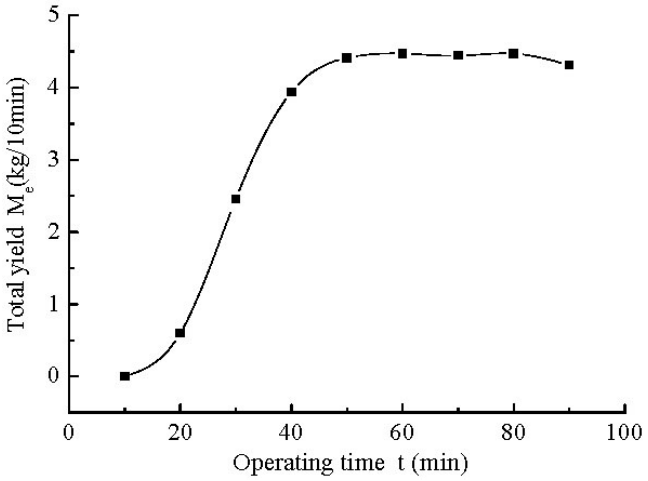

Fig. 2. Variations of the total yield measured at 10-min intervals of operating time.

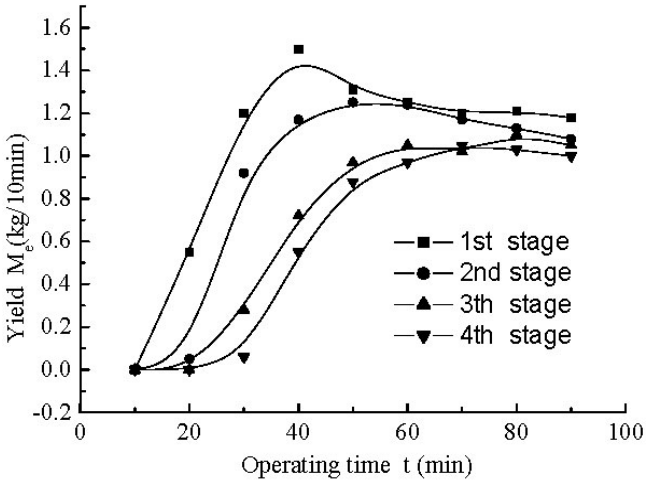

Fig. 3. Variations of the yields in different stages measured at 10-min intervals of operating time

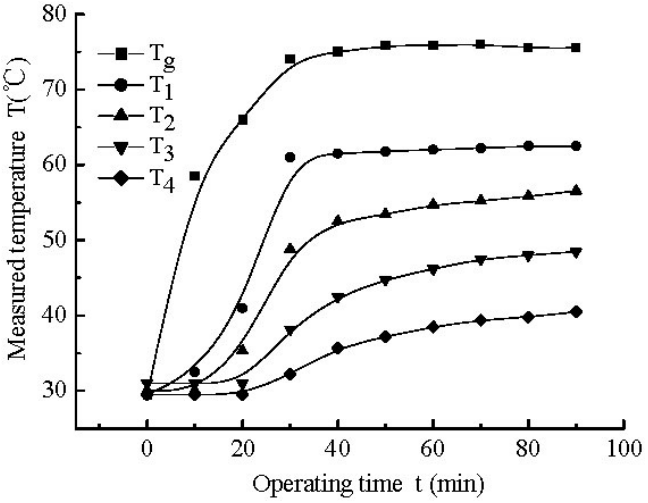

Fig. 4. Variation curves of the temperatures with transient state operating time.

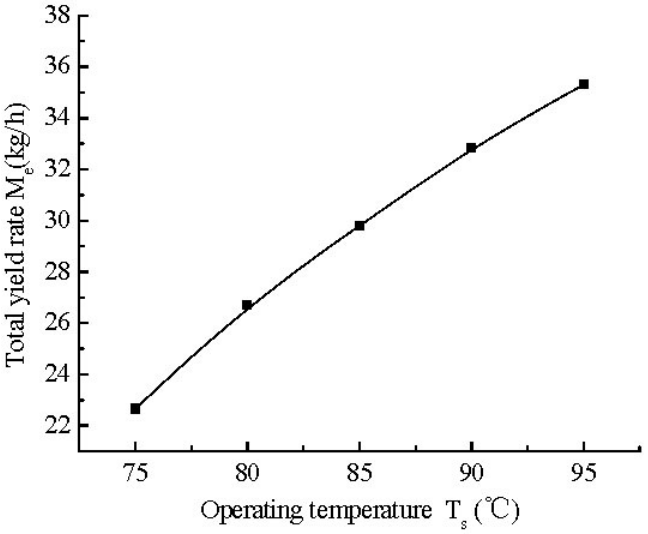

Fig. 5. Influence of the operating temperature of the system on the fresh water yield.

$$M_e = 49.05 - 252.38 \Big/ \left[1 + \exp\left(\frac{T_s - 13.96}{24.40}\right)\right] \quad (1)$$

The vapor temperature variations with the operating temperature under the forementioned operating conditions are shown in Fig. 6. It is shown that the temperatures of vapors in generator and the fourth stage evaporator are highest and lowest, respectively. But both of them increase with a rise of the operating temperature. On the other hand, the difference between T_g and T_1 is largest. That of T_3 and T_4 is the next. The larger difference between T_g and T_1 may be explained as follows. Firstly, because the saturated vapor pressure of lithium bromide is less than that of water at the same temperature, then T_g has to be higher so as to drive the vapor from the generator to the first stage evaporator. Secondly, the diameter of the vapor pipe connecting the generator and the first stage evaporator may be relatively small, which increases the resistance of vapor flow. That the saturated vapor pressure of lithium bromide is less than that of water at the same temperature can explain the larger difference between T_3 and T_4 in the same way. The same explanation can interpret the phenomenon why the lithium bromide in the absorber can absorb the vapor in the fourth stage evaporator, which makes the fourth stage evaporator operate at lower temperature and the latent heat of vapor recycled in the last stage evaporator and can intensify the processes of evaporation and condensation in preceding stage evaporator so as to raise the heat utilization of the system.

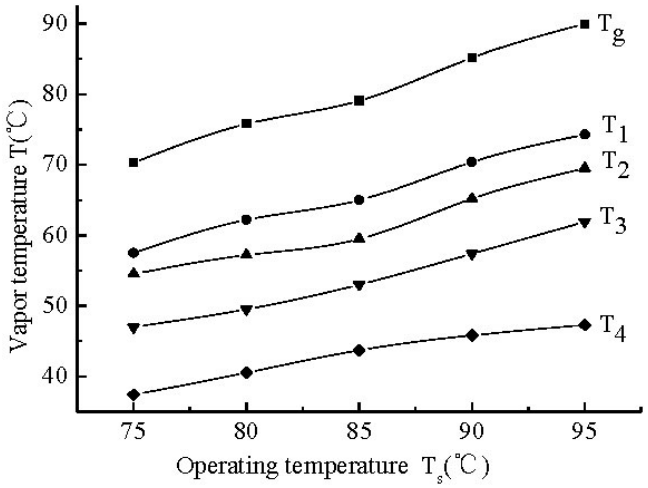

Fig. 6. Variations of the vapor temperature with operating temperature in different parts.

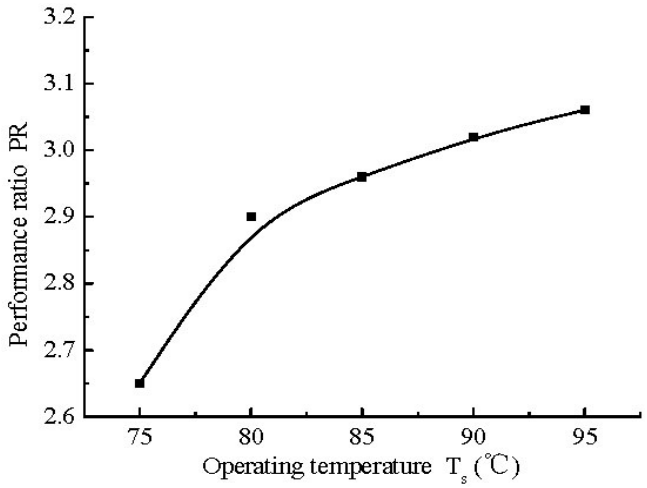

Fig. 7. Influence of the operating temperature of the system on the performance ratio.

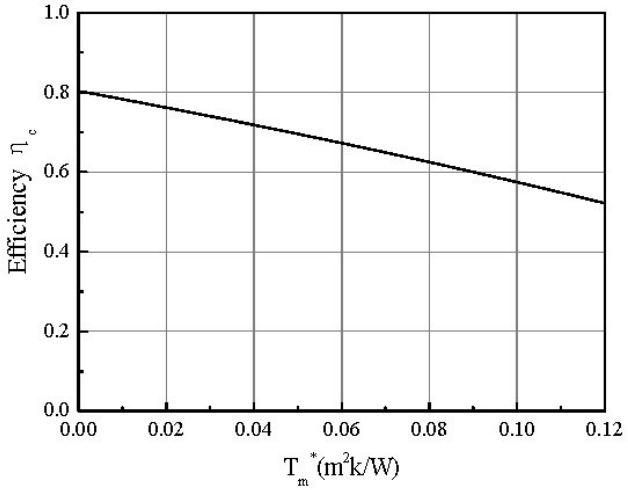

Fig. 8. Efficiency curve of the solar collector with respect to absorber area.

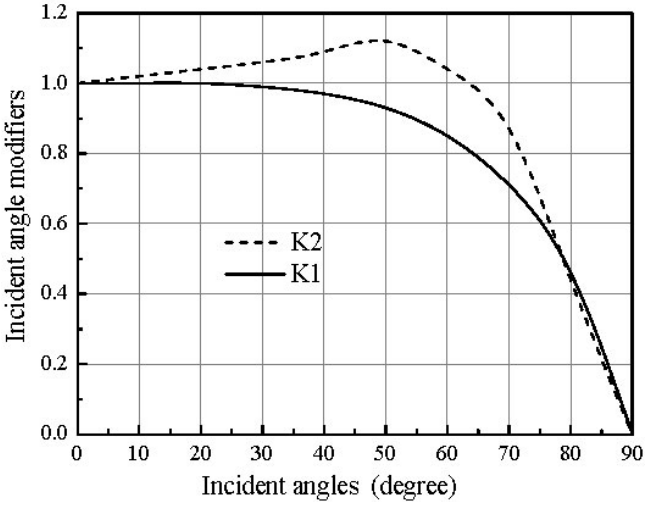

Fig. 9. Variation curves of the longitudinal and transversal incident angle modifiers of solar collector with the incident angles.

The performance ratio (PR) reflects the performance of the system. It is defined as follows.

$$PR = \frac{M_e h_{fg}}{E} = \frac{M_e h_{fg}}{Q + 3.6P_s} \quad (2)$$

where Δt is the time interval of the pumps operation.

As shown in Fig. 7, the variation curve of performance ratio with operating temperature is given and it is seen that the performance ratio of the system is relatively high while the operating temperature is 80–90°C. The performance ratio increases with the increase of operating temperature when the other operating conditions remain unchangeable. It is said that the system possesses more advantages at higher operating temperature. Compared to the conventional multiple effect system [11] with the same number of effects and under the same operating conditions, it is found that the PR of the system was not much bigger than that of the conventional multiple effect system when the temperature is less than 90°C. However, when the operating temperature is higher than 90°C, the PR of the system is obviously bigger than that of the system in Li et al. [11].

It was also found through the experiment that many factors, especially the operating pressure and the flow rate of brine, influence the system's performance ratio. Lower operating pressure is favorable to evaporation and is also helpful to increase the performance ratio of the system. The condensed and ejected brine will take part of sensible heat off the system. Hence, the performance ratio of the system generally increases when the flow rate of brine decreases. But considering the crystallization, it would be

better that the flow rate of brine is adjusted to 1.5–2.0 times that of fresh water.

The equation of the variation curve of PR with operating temperature shown in Fig. 7 can be fitted as follows:

$$PR = \begin{cases} -23.9 + 0.639T_s - 0.0038T_s^2 & 60 \le T_s < 80 \\ 0.515 + 0.0458T_s - 0.0002T_s^2 & 80 \le T_s \le 115 \end{cases} \quad (3)$$

6. Optimal parameters for the solar heating system

The proposed solar heating system, which is shown in Fig.1, is constructed with the solar collectors, hot water storage, circulation pump and other components. The solar collectors are evacuated tube collectors (Sunda) which were test by the Test Center Institute für Solartechnik SPF in Switzerland. As shown in Figs. 8 and 9, the curves of the efficiency and the longitudinal and transversal incident angle modifiers of the collector are presented. The equation of efficiency curve could be expressed as:

$$\eta_c = 0.803 - 2.01T_m^* - 0.0034G_tT_m^{*2} \quad (4)$$

where

$$T_m^* = \frac{T_{mc} - T_a}{G_t} \quad (5)$$

During the simulation, the hourly beam and diffuse irradiance of 2003 in Beijing and the following models are used:

1. The hourly irradiance changes linearly or evenly within 1 h.
2. The dimensions of the hot water storage vary with the volume according to a definite correlation, but the material and thickness of the heat insulation remain unchangeable.
3. The fluids from the solar heating system and the generator are completely mixed after entering the hot water storage.
4. The ambient temperature is the daily average temperature.
5. The heat losses of the pipes are neglected.
6. The physical processes, when the operation of the absorption desalination system changes from one state to another, are taken as quasi-steady-state processes.
7. The operating parameters and conditions of the absorption desalination system are the same as those in the steady state experimental study mentioned above.

When the solar collectors absorb the irradiance and transform it into heat, the collector fluid is heated and pumped into the hot water storage. It is controlled by a solar controller. If the temperature of the fluid in the storage reaches a start-up temperature, the fluid is pumped to the absorption desalination system to produce freshwater (see Fig. 1). According to the above model, the heat equilibrium equation of the storage due to the time t can be expressed as

$$\left(m_cc_p\right)\left(T_{ic} - T_{oc}\right) + \left(M_sc_p\right)\left(T_o - T_s\right) - Q_L = 3600\,\rho_w V_t c_p \frac{\mathrm{d}T_s}{\mathrm{d}t} \quad (6)$$

Neglecting the heat losses and by Eq. (2), the following equations are obtained:

$$\left(m_cc_p\right)\left(T_{is} - T_s\right) = Q_c \quad (7)$$

$$\left[\left(M_sc_P\right)\left(T_o - T_s\right) + 3.6P_s\right]PR = M_eh_{fg} \quad (8)$$

where the value of P_s is 1300 W.

The energy Q_c gathered by solar collectors can be estimated by the following formula:

$$Q_c = 3.6K_1K_2A_cG_t\eta_c \quad (9)$$

where η_c can be calculated by Eq. (4) and the total irradiance G_t, which can be calculated by the beam and diffuse irradiances [12].

If the lifetime and cost of the solar desalination unit, the electricity fee and the yield of the unit operating a year are given, respectively, then the cost of fresh water per cubic meter can be calculated by the following equation:

$$P_{co} = \left(F_s / L_t + F_e\right) / M_{et} \quad (10)$$

where the value of F_s and L_t are \$2400 and 15 years, respectively. F_e varies with the A_c and V_t. But the electricity fee is 0.07 (\$ $kw^{-1}h^{-1}$).

Because the solar radiation changes all the time, a definite value of the storage volume is required to assure that the solar desalination unit can continuously operate a period of time. For this reason, it is considered that when the operating temperature T_s reaches the temperature called start-up temperature T_{st}, the desalination unit starts to operate until T_s decreases to the "break" temperature (T_{br}), and the unit stops operating temporarily. Once T_s is equal to or greater than T_{st}, the unit starts to operate again and will stop while T_s is equal to or smaller than T_{br}. The desalination unit continuously repeats the start-up and break operating actions depending on the value of T_s. If

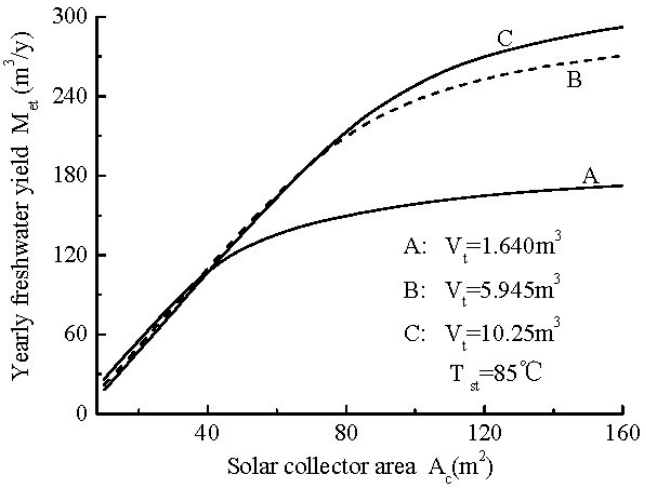

Fig. 10. Variation curves of the annual yield of fresh water with the area of solar collectors.

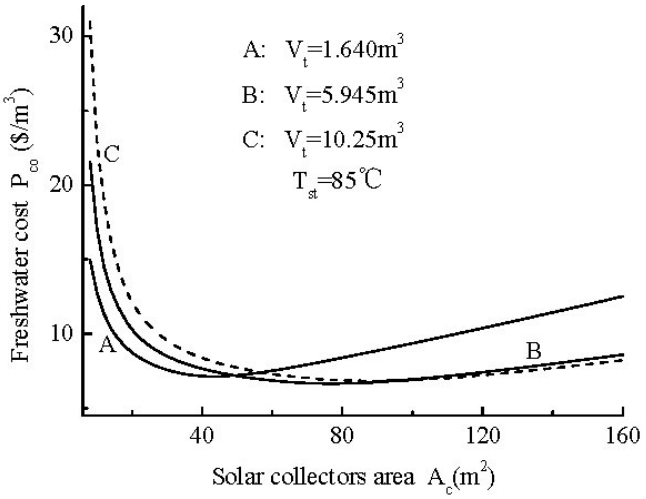

Fig. 11. Variation curves of the cost of fresh water production with the area of solar collectors.

the temperatures of T_{st} and T_{br} are set to be 85°C and 75°C, respectively, the variations of the M_{et} and P_{co} with A_c with respect to different volume values of the storage can be seen in Figs. 10 and 11.

As shown in Fig. 10, M_{et} increases with a rise in A_c, and it is found that there exists a value called A_0. While A_c is less than A_0, M_{et} rises fast. But while A_c is larger than A_0, M_{et} increases more and more slowly. It can be explained as follows: Firstly, when the volume of the storage is a definite fixed value and A_c is less than A_0, it is obvious that the rise in A_c makes the temperature of the fluid in the storage achieve the start-up temperature T_{st} more easily under different irradiation conditions and the operation of the unit will last much longer. Therefore, M_{et} increases fast with a rise of A_c. Secondly, when A_c is larger than A_0, the operating temperature of the unit can reach T_{st} in most of days with better irradiation. However, if A_c is large enough to increase the temperature over 115°C on some days, some of the fluid in the storage will be released so as to maintain the temperature of the storage not greater than 115°C. This will result in heat waste. And the kind of heat waste would increase with a rise of A_c. Hence M_{et} will increase more and more slowly when A_c becomes larger and larger.

It can also be seen in Fig. 10 that there is an intersection of the curves with small V_t and larger V_t. If the area value correspondent to the point be A_1, it is found that the smaller the A_c, the higher the M_{et}, while A_c is smaller than A_1. However, when A_c is larger than A_1, the larger the A_c, the higher the M_{et}. This can be explained as follows. Firstly, it is easier to achieve T_{st} and produce fresh water with a rise of A_c for the unit with the smaller V_t when A_c is less than A_1. Secondly, when the A_c is larger enough and larger than A_1, it is easier for the unit to reach the limited temperature (115°C) and waste heat with smaller V_t. But

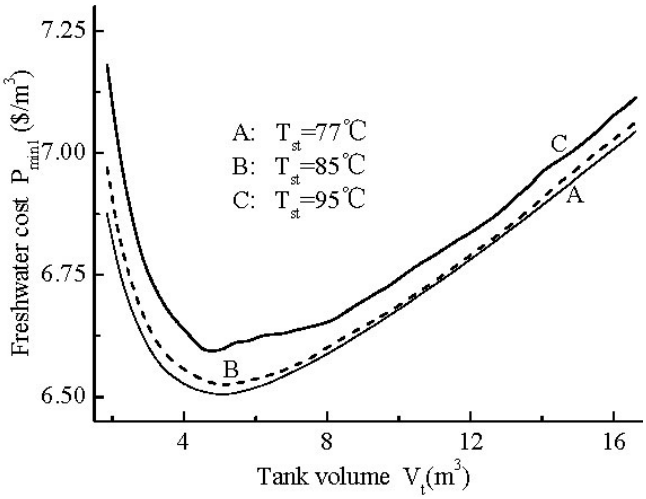

Fig. 12. Variation curves of P_{min1} with storage volume.

the unit with larger V_t may last much longer time to operate with higher T_s and produce more fresh water than a smaller V_t does.

When V_t and other parameters are fixed, P_{co} varies with the change of A_c, but there is a minimum called P_{min1}, which is shown in Fig. 11. When A_c is less or greater than the value of the correspondent area to P_{min1}, its correspondening P_{co} is always higher than P_{min1}. This can be interpreted as follows: higher P_{co} is the result of the temperature of the fluid in the storage being lower while A_c is less, which will make the unit produce less fresh water or even none. But with the rise of A_c, the temperature of the fluid in the storage will increase, which makes M_{et} increase too and P_{co} is reduced. However, if A_c continues to increase after P_{co} has achieved P_{min1}, a higher temperature of the fluid in the storage will cause an increase of the heat waste due to the limited temperature

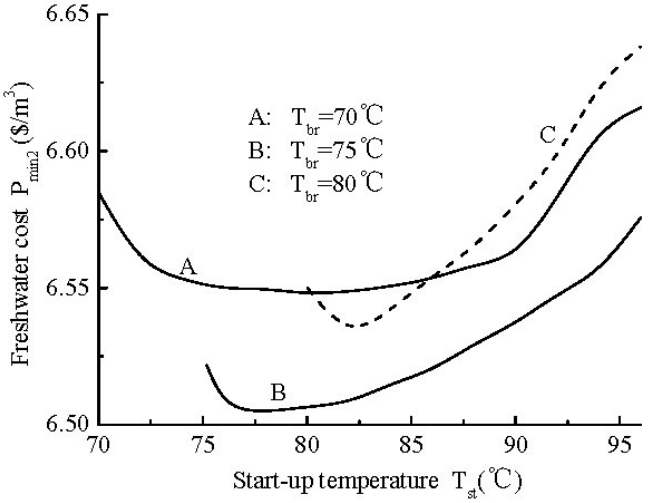

Fig. 13. Variation curves of P_{min2} with T_{st}.

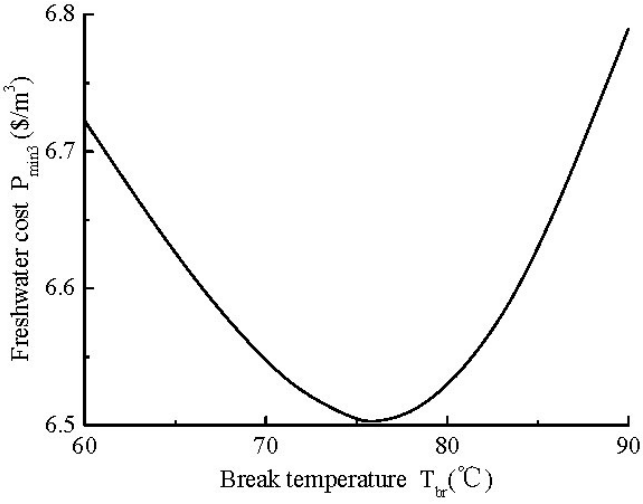

Fig. 14. Variation curve of P_{min3} with T_{br}.

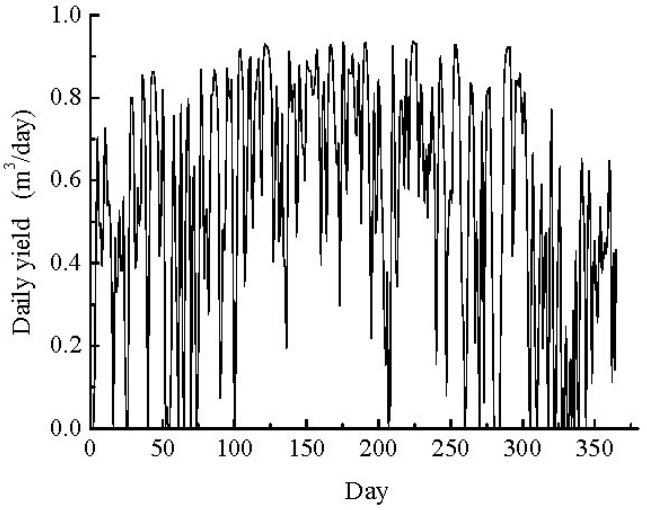

Fig. 15. Variation curve of the daily yield of fresh water with the day.

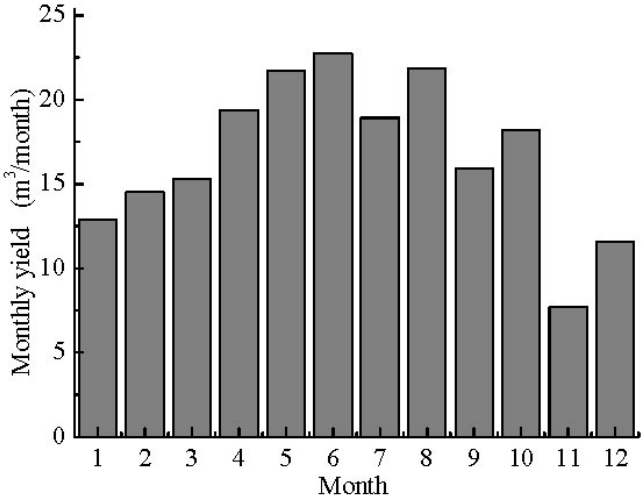

Fig. 16. Variation of the monthly yield of fresh water with the month.

confinement. It can also be seen in both Figs. 10 and 11 that If V_t is fixed and A_c is equal to A_0, the correspondent P_{co} achieves the minimum.

It is seen in Fig. 12 that P_{min1} changes with different V_t. Therefore, the study on the correlation between P_{min1} and V_t would be helpful to acquaint the unit with the performances. Let the break temperature be 75 and alter T_{st}. The variation curves of P_{min1} with V_t are shown in Fig.12.

As shown in Fig. 12, there is a minimum in each curve but the minimum of P_{min1} varies with T_{st}. If the minimum of P_{min1} is defined as P_{min2}, then the correspondent values of V_t and A_c to P_{min2} are the optimal parameters of the unit at T_{st}.

As shown in Fig. 13, P_{min2} changes with different T_{st} while T_{br} is fixed. Also there is a minimum, which is called P_{min3}, in each curve. It can be seen that when the start-up temperature is not equal to the T_{st} corresponding to P_{min3}, P_{min2} is higher than P_{min3} at all times. Also it could be seen that P_{min3} changes with T_{br}. Therefore, it is better to study the variation correlation between P_{min3} and T_{br} to investigate the parameters of the solar heating system of the unit. The results of the investigation demonstrate the variation curve of P_{min3} and T_{br}, shown in Fig. 14. It is similarly found that there is a least value called P_{min4} in the curve.

Through the above study, it is obvious that the T_{st}, T_{br}, V_t and A_c, which are correspondent to P_{min4}, are the optimal parameters of the absorption solar desalination system. It can also be seen that the value of P_{min3} changes very slowly. Hence there should be a reasonable scope for optimal parameters of the system within a certain relative deviation.

From the above analysis, the optimal parameters of the system correspondent to P_{min4} are determined, which are 73.34 m^2 solar collectors, 5043 L storage volume, 78°C start-up and 76°C break temperatures, as simulated by the irradiance and daily mean ambient temperature of 2003 in Beijing. Then the annual yield is about 201 m^3. The variation curves of daily and monthly yields of fresh water with day and month are shown in Figs. 15 and 16.

7. Conclusions

Low-temperature absorption solar desalination with quadruple effect regeneration was designed and tested indoors under steady-state heating conditions. The unit operated steadily and the yield rate was high. The yield rate could achieve 30 kg/h at 80–90°C operating temperature.

The unit possesses more advantages when it operates at higher temperatures and lower pressure. But when the operating temperature and pressure are 70–90°C and 8–20 kPa respectively, the influence of the flow rates of hot and cooling water is not obvious and the unit could operate normally in the scopes of 0.6–2.5 and 0.5–1.5 m^3/h.

Based on the steady-state experiment and the beam and diffuse irradiance data, the optimal parameters of the solar heating system can be calculated by simulating the actual system operation under the conditions of the least cost of fresh water.

If the solar collectors have a slope of 33° due south, according to the irradiance of 2003 in Beijing, and the parameters are 4.5–5.6 m^3 storage volumes, 63–80 m^2 solar absorber areas, 74°C break temperature and 79°C start-up temperature, the cost of fresh water would be the least and change within 2%. The above results are concluded from the city water. Therefore, the effects of the salinity and the scale on the calculation results by using the model should be considered when seawater is applied to the experimental unit.

8. Symbols

A_c — Solar collector area, m^2
c_p — Specific heat of water, kJ kg^{-1} $^{-1}$
E — Total energy consumed by the system, kJ h^{-1}
F_e — Annual electrical cost, y^{-1}
F_s — Cost of the solar desalination unit
h_{fg} — Heat of vaporization of water, kJ kg^{-1}
G_t — Global irradiation, W m^{-2}
K_1 — Longitudinal incident angle modifier
K_2 — Transversal incident angle modifier
L_t — Lifetime of the unit, y
m_c — Flow rate of collector fluid, kg h^{-1}
M_e — Fresh water yield rate of the unit, kg h^{-1}
M_{et} — Annual fresh water yield of the unit, m^3 y^{-1}
M_s — Hot water flow rate, kg h^{-1}
P_{co} — Cost per cubic meter, m^{-3}
$P_{min1–4}$ — Minimum cost of fresh water in Figs. 11–14 respectively, m^{-3}
P_s — Total electric power, W
PR — Performance ratio of the unit
Q — Thermal energy rate inputted into the desalination system, kJ h^{-1}
Q_c — Thermal energy rate collected by solar collectors, kJ h^{-1}
Q_L — Heat loss rate of the pipe lines, kJ h^{-1}
t — Time, s
$T_{1–4}$ — Temperature in measuring point shown in Fig. 1, °C
T_a — Ambient temperature, °C
T_{br} — Break temperature, °C
T_g — Vapor temperature in generator, °C
T_h — Inlet temperature of sea water in absorber, °C
T_{ic} — Inlet temperature of solar collectors, °C
T_{is} — Inlet temperature of the storage, °C
T_L — Temperature of lithium bromide solution in absorber, °C
T_{mc} — Mean temperature of solar collectors, °C
T_m^* — Reduced temperature, m^2 K w^{-1}
T_o — Outlet temperature in generator, °C
T_{oc} — Outlet temperature of solar collectors, °C
T_s — Inlet or operating temperature in generator, °C
T_{st} — Start-up temperature of the unit, °C
V_t — Volume of the storage, m^3

Greek

η_c — Efficiency of solar collector
ρ_w — Density of water, kg m^{-3}

Acknowledgement

Thanks are due for the financial support from the National Natural Foundation of China (No. 50576004) and the meteorological data supplied by the National Meteorological Information Center.

References

[1] N.X. Tsiourtis, Desalination and the environment. Desalination, 141 (2001) 223–236.
[2] H. Zheng, K. He and Z. Chen, Solar Desalinization Technology. of Beijing Institute of Technology Press, Beijing, 2005.

[3] J. Weimberg, A. Ophir and U. Fisher, Coupling of multi-effect distillation with vacuum freezing to reduce energy cost in seawater desalination. Proc. 7th Int. Symp. on Fresh Water from the Sea, 1 (1980) 283–292.
[4] K. Fatbalah and S.E. Aly, Theoretical study of a solar powered absorption/MED combined system. Energy Conv. Mngmt., 31 (1991) 529–544.
[5] F. Al-Juwayhel, H. El-Dessouky and H. Ettouney, Analysis of single-effect evaporator desalination systems combined with vapor compression heat pumps. Desalination, 114 (1997) 253–275.
[6] H.T. El-Dessouky and H.M. Ettouney, Fundamentals of Salt Water Desalination, Elsevier, New York, 2002.
[7] L. García-Rodríguez and C. Gómez-Camacho. Thermoeconomic analysis of a solar parabolic trough collector distillation plant. Desalination, 122 (1999) 215–224.
[8] A..M. El-Nashar, Validating the performance simulation program "SOLDES" using data from an operating solar desalination plant. Desalination, 130 (2000) 235–253.
[9] L. García-Rodríguez, A.I. Palmero-Marrero and C. Gómez-Camacho, Thermoeconomic optimization of the SOL-14 plant (Plataforma Solar de Almeria, Spain). Desalination, 136 (2001) 219–223
[10] A.M. El-Nashar, Optimizing the operating parameters of a solar desalination plant. Solar Energy, 48 (1992) 207–213.
[11] Z. Li, H. Zheng, Z. Chen, K. He, J. Fang and M. Xie, Experimental studies on a low temperature multi-effect solar desalination system with falling film evaporation. Taiyangneng Xuebao/Acta Energiae Solaris Sinica, 28 (2007) 421–426.
[12] J.R. Simonson, Computing Method in Solar Heating Design, Macmillan, New York, 1984.